Journal of Asian Earth Sciences 37 (2010) 207–218

Contents lists available at ScienceDirect

Journal of Asian Earth Sciences

journal homepage: www.elsevier.com/locate/jseaes

A-type granite of the Hasan Robat area (NW of Isfahan, Iran) and its tectonic significance

M. Mansouri Esfahani [a,*], M. Khalili [b], N. Kochhar [c], L.N. Gupta [c]

[a] Department of Mining Engineering, Isfahan University of Technology, Isfahan, Iran
[b] Department of Geology, The University of Isfahan, Isfahan, Iran
[c] CAS in Geology, Punjab University, Chandigarh 160 014, India

ARTICLE INFO

Article history:
Received 27 November 2007
Received in revised form 18 May 2009
Accepted 21 May 2009

Keywords:
A-type granite
Rift tectonic
Hasan Robat Granite
Sanandaj–Sirjan Zone
Iran

ABSTRACT

The Late Precambrian Hasan Robat Granite occurs in the northwestern part of the Sanandaj–Sirjan Zone NW of Iran. The granitoid rocks are composed of biotite-bearing syenogranite, alkali-feldspar granite and minor amount of monzogranite. The main minerals are quartz, microcline, plagioclase (albite–oligoclase), green biotite, and amphibole (ferrohornblende) with subsolvus to subordinate hypersolvus affinities.

Chemically, the rock suite is characterized by high SiO_2, Fe/Mg, total alkali (K_2O, Na_2O), Zr, Nb, Y, Hf, Ta, Ga/Al, and REE (except for Eu), and low contents of MgO, CaO, P_2O_5, and Sr. They display A-type characteristics, being ferroan, alkali–calcic to calc–alkalic and metaluminous to peraluminous with minor of peralkaline nature. Crystallization of such magmas has produced the iron-enrichment and alkali composition of the Hasan Robat Granite which likely occurred in an extensional environment. Low abundances of Ba, Sr, P, Ti, Eu, the positive correlation between Ba and Eu anomalies, and the negative correlation between Rb and K/Rb reveal fractional crystallization of alkali feldspar produced at the final compositions of these granites. The low ratios of Y/Nb (<1.2) as well as the ferroan composition of these rocks suggest that they are fractionation from mantle derived magma related to Within Plate Granite (WPG) field.

Crown Copyright © 2009 Published by Elsevier Ltd. All rights reserved.

1. Introduction

The Sanandaj–Sirjan Zone (SSZ) with a NW–SE orientation, is a part of Zagros orogen (Alavi, 1994), and is considered as an aborted rift (Rashidnejad-Omran et al., 2002). The belt with 1500 km length, and a width of approximately 200 km, consists of metamorphic complexes of deformed rocks in association with widespread deformed and undeformed plutonic as well as Mesozoic volcanic rocks (Shabanian et al., 2009) (Fig. 1). For the past 40 years, the occurrence of numerous granitic plutons in the SSZ has been under extensive geological investigations.

Thiele et al. (1968) identified three different magmatic events in the Golpayegan area (about 50 km west of the study area) (Fig. 1). The first event which is the oldest one (Late Precambrian) is characterized by three plutonic bodies viz. (i) The Muteh Granite, (ii) the Hasan Robat Granite, and (iii) the granites occurring in the northern area of Golpayegan city. The second event, consisting predominantly of biotite granodiorite to granite, is located near Aligudarz city (about 80 km west of Hasan Robat Granite). These rocks intruded into a Jurassic shale–sandstone sequence displaying either crustal origin (e.g. Muteh, Azna and Kolah-Ghazi Granites) (Othrody, 1988; Tabatabaei-Manesh, 1994; Noghreian and Tabatabaei-Manesh, 1995; Khalili and Khalili, 2002; Moazzen et al., 2004), or crustal-mantle origin (e.g. Aligudarz Granites) (Bagherian and Khakzad, 2001) and are genetically linked to syn-collisional and post-orogenic tectonic settings. The third episode which is predominantly diorites and gabbro–diorites intruded into the marl–shale sequence of upper Cretaceous. According to some authors (Turkian, 2008; Tahmasebi, 2009) the granitoid rocks exposed in the south of Qorveh and Astaneh are most commonly classified as volcanic arc granite (VAG) related likely to active continental margin. Recently, a number of workers (Mansouri Esfahani, 2003; Sepahi and Athari, 2006; Davoudian et al., 2007; Shabanian et al., 2009) reported the anorogenic and/or post-orogenic alkaline granites (A-type) from several localities (Hasan Robat, Saqqez, Golpayegan and Ghaleh-Dezh) in the Sanandaj–Sirjan structural zone.

For the purposes of the present study we use field relationships, petrography as well as major and trace element chemistry to constrain the petrogenesis and tectonic setting of the Hasan Robat Granitic magma. The area under investigation is situated about 140 km northwest of Esfahan (Fig. 2).

2. Field relations

The Hasan Robat Granite lies between 50°45′–51°00′ longitude and 33°15′–33°30′ latitude and is located in the central part of the

* Corresponding author.
E-mail address: mmansouri_2001@yahoo.com (M.M. Esfahani).

1367-9120/$ - see front matter Crown Copyright © 2009 Published by Elsevier Ltd. All rights reserved.
doi:10.1016/j.jseaes.2009.05.010

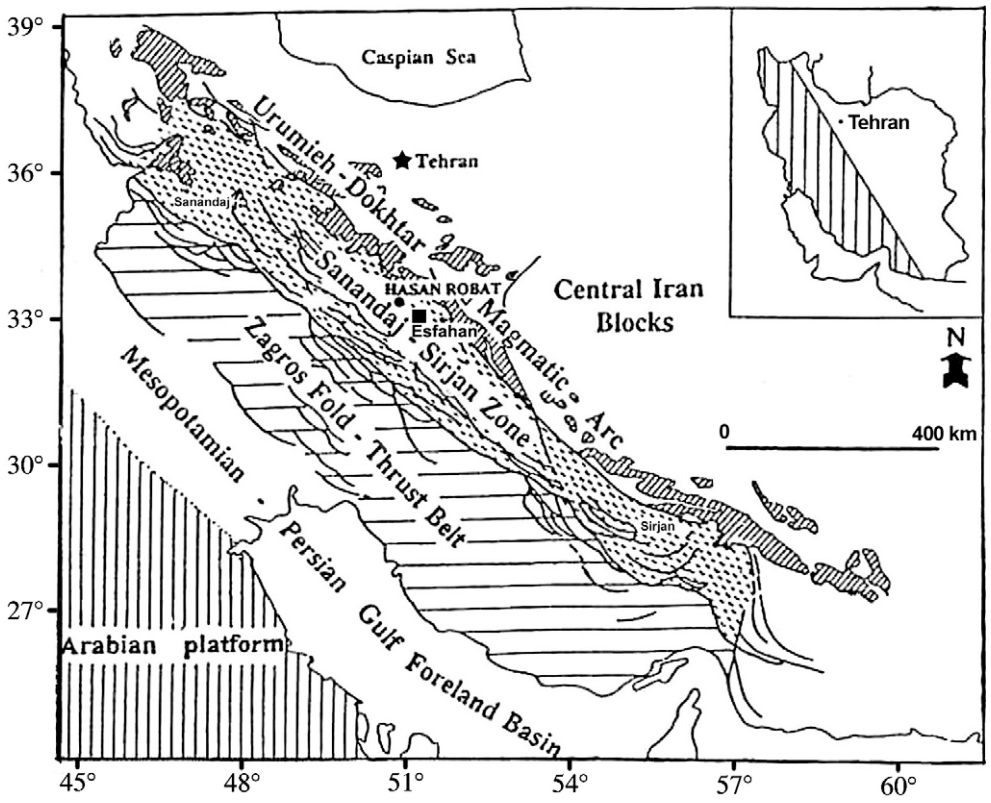

Fig. 1. Tectonic zones of the Zagros orogen (after Alavi (1994)).

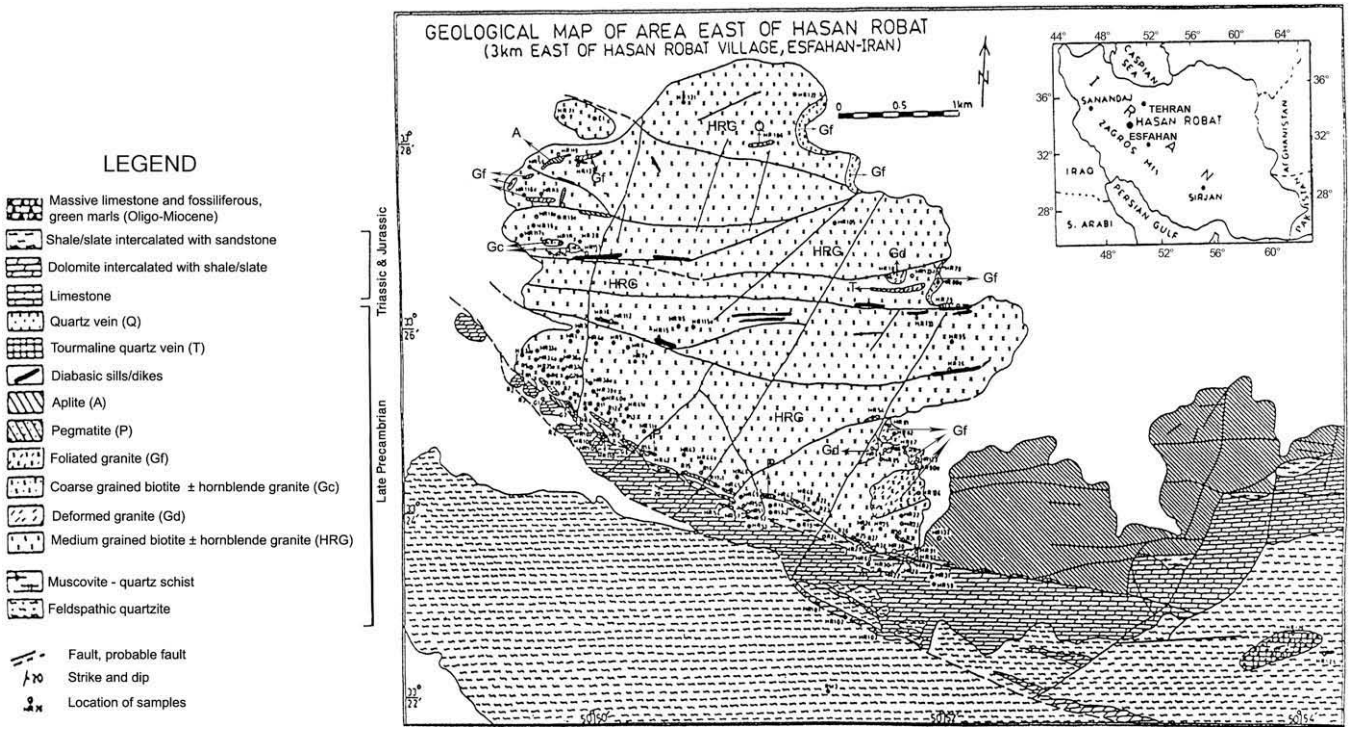

Fig. 2. Geological map of the Hasan Robat Granite.

SSZ (Fig. 1). Most of the rocks of under investigation are medium-grained, 2 mm to 2 cm in size. The rocks are creamy white to light gray in color. Towards the northern and eastern sides, the granite becomes relatively coarse-grained and gradually grades into granite porphyry at the pluton margin. Fine to medium aplites as massive or veins, are observed within or adjacent to the main pluton.

The country rocks are: (i) muscovite-quartz schist; (ii) biotite schist; and (iii) feldspathic quartzite. The latter two also occur as

xenoliths. The biotite schist xenoliths are rounded to elliptical in shape. They, locally form a fine- to medium-grained mixed facies with the granitic rocks. The feldspathic quartzite xenoliths occur as thin tabular masses in the southwest to southeasternmost part of the Hasan Robat Granite body. A zone rich in xenoliths defines the marginal zone of the granitic mass. These xenoliths have inherited their own characteristics from the country rocks.

Hornblende-biotite granites are found as enclaves in the studied rocks. They range from elliptical to rounded shape with dark gray color and have a sharp contact with the host granite. Chemically, the enclaves are similar to the host granitic rocks and probably represent fragments of the early-crystallized portions of host magma which have been incorporated in the granitic body (Mansouri Esfahani and Khalili, 2007).

3. Petrography

3.1. Granite

The predominant granitic rocks of the Hasan Robat Granite are syenogranite and alkali-feldspar granite with rare monzogranite (Streckeisen, 1979) (Fig. 3). They are typically medium- to very coarse-grained with quartz, K-feldspar (mostly microcline), plagioclase (albite), biotite and ±hornblende and have predominately porphyritic texture. The phenocrysts are composed of quartz, feldspar and biotite.

The granitic rocks are mainly subsolvus in nature, but a minor component of hypersolvus granite with ferrohornblende and acmite in the norm also occur (Mansouri Esfahani, 2003). The Hasan Robat Granites are composed of several intergrowth textures including perthite, myrmekite, graphic, rapakivi, and albite rims over plagioclase. Perthitic and granophyric textures are more common in the samples having ferrohornblende. Medium-grained quartz with anhedral to subhedral shape occurs in interspaces between K-feldspar, plagioclase and biotite. It shows undulatory extinction in most samples.

Medium- to very coarse-grained K-feldspar is present as laths and frequently containing inclusions of quartz and plagioclase. Larger crystals of K-feldspar are embedded in finer-grained groundmass exhibiting porphyritic texture. Development of thin films in albite is often observed in the microcline giving rise to braided, patched perthite and microperthite texture.

Plagioclase (albite to oligoclase, An_{28}) is usually subhedral to rarely anhedral and is medium- to coarse-grained. It shows albite twinning. Myrmekite texture is developed at the margins of plagioclase and microcline. Worm-like or finger-like or droplets of quartz are enclosed in oligoclase. Fine- to coarse-grained biotite is the principal mafic mineral in the studied granites. It shows pleochroism from greenish yellow to green color and is often altered to chlorite and opaque minerals.

Bluish green to green hornblende (Z^C = 33°) in medium-grained grain size occurs as relict mineral in association with biotite. It is commonly replaced by biotite and chlorite as well as calcite, epidote, titanite and opaques. In some hornblendes relicts of pyroxene are still preserved.

Accessory phases including apatite, zircon, titanite, opaques and allanite are present. Allanite is generally subhedral to anhedral and is pleochroic from red to brownish red. Occasionally, allanite is zoned and may be rimmed by clinozoisite. Zircon is usually idiomorphic and is enclosed in biotite and feldspars. Granular or ellipsoidal titanite formed during the alteration of hornblende to biotite and chlorite.

3.2. Aplite and pegmatite

The main minerals in the aplite are quartz, K-feldspar, sodic plagioclase, ±muscovite. These rocks mineralogically, are similar to the Hasan Robat Granite except for more quartz and sodic plagioclase and less biotite and hornblende. Traces of accessory fluorite are observed in a few samples (Mansouri Esfahani, 2003). Pegmatites are intimately associated with aplite and quartz veins. They are light grayish pink or pinkish white in color with similar minerals to those of the granites. Sometimes very coarse-grained tourmaline and feldspars both with over 15 cm in length are present.

3.3. Diabase rocks

The diabase sills/dikes cut the Hasan Robat Granite and are represented by dolerite and metamorphosed diabase. They are fine- to coarse-grain and are essentially composed of plagioclase (An_{46}),

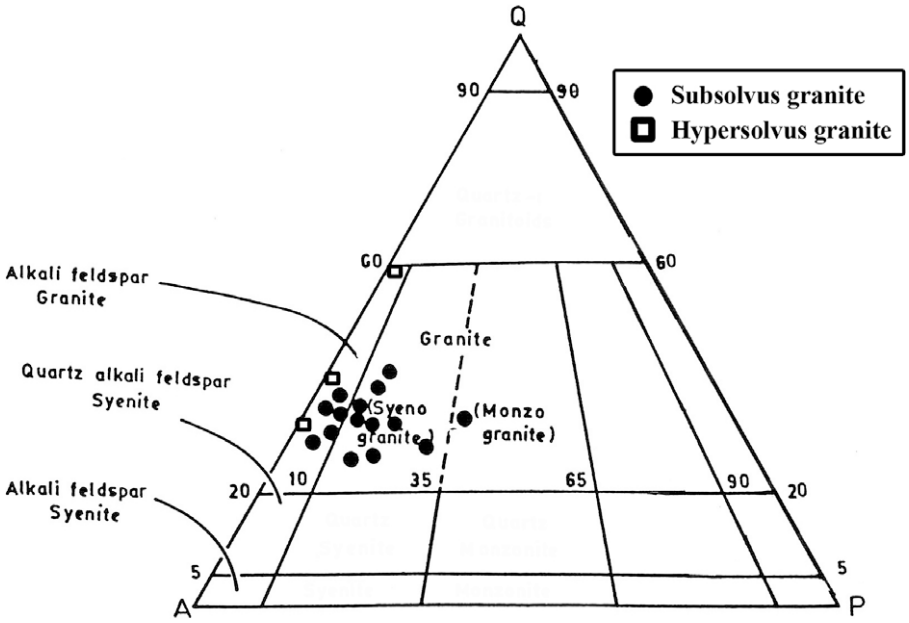

Fig. 3. The Hasan Robat Granites in the QAP triangular diagram (Streckeisen, 1979).

Table 1
Chemical analyses of the Hasan Robat Granite.

	Subsolvus granites														Hypersolvus granites		
Sample No.	HR24	R10	R13	HR119	HR6	HR22	HR122	R22	HR113	HR121	HR115	HR86	R7	HR71	HR124	HR61	HR18
Oxide wt.%																	
SiO_2	70.16	70.79	70.82	71.01	71.24	71.69	71.85	71.95	72.51	72.51	73.16	74.10	74.92	75.36	75.41	77.36	80.12
TiO_2	0.17	0.16	0.32	0.24	0.16	0.54	0.31	0.34	0 .24	0.30	0.22	0.20	0.05	0.23	0.13	0.15	0.21
Al_2O_3	13.38	14.4	14.20	13.28	11.96	10.32	12.77	13.34	12.43	12.98	12.92	12.34	12.89	11.65	12.27	10.61	8.66
Fe_2O_3	0.22	0.17	0.30	2.22	1.98	0.82	2.18	0.34	2.06	2.40	2.07	0.23	0.16	0.33	1.42	0.23	0.28
FeO	1.5	1.14	2.05	0.30	0.29	5.49	0.30	2.30	0.30	0.35	0.30	1.56	1.10	2.20	0.20	1.54	1.90
MnO	0.02	0.02	0.04	0.05	0.03	0.10	0.04	0.03	0.05	0.05	0.04	0.04	0.02	0.04	0.02	0.02	0.03
MgO	0.12	0.53	0.49	0.28	0.15	0.48	0.51	0.32	0.42	0.29	0.21	0.96	0.16	0.10	0.16	0.06	0.17
CaO	0.72	1.22	1.10	1.09	0.69	2.05	0.73	0.72	0.96	1.19	1.17	1.12	0.46	1.23	0.60	0.92	0.75
Na_2O	3.13	4.92	3.93	3.37	3.22	3.02	3.73	2.98	3.37	3.36	3.64	3.37	2.87	3.31	3.65	3.37	2.79
K_2O	5.06	2.67	4.64	5.03	4.48	3.84	5.39	5.41	4.80	4.55	5.84	4.94	5.27	4.48	5.88	4.81	4.66
P_2O_5	0.07	0.04	0.09	0.08	0.07	0.18	0.10	0.08	0.07	0.10	0.05	0.03	0.03	0.05	0.04	0.10	0.05
LOI	0.98	0.95	0.95	0.95	0.98	0.56	0.88	0.99	0.98	1.32	0.08	0.92	2.04	1.02	0.05	0.83	0.38
Total	95.53	97.05	98.93	97.9	95.35	99.09	98.79	98.8	98.19	99.40	99.70	98.86	99.97	98.98	99.83	99.17	99.62
Ratios																	
Na/K	1.06	0.35	0.82	1.06	0.90	0.85	0.95	1.20	0.93	0.88	1.07	0.96	1.22	0.97	1.07	0.94	1.25
KN/C	8.60	5.10	5.70	5.67	8.00	2.60	9.00	8.20	3.00	5.10	16.00	5.30	12.40	5.00	11.20	6.60	6.90
A/CNK	1.13	1.10	1.09	1.00	1.00	0.79	0.96	1.10	1.00	1.04	0.86	0.95	1.14	0.91	0.90	0.86	0.77
A.I.	0.77	0.76	0.78	0.85	0.85	0.90	0.95	0.81	0.85	0.80	0.95	0.90	0.81	0.90	1.02	1.01	1.10
Trace elements (ppm)																	
Ba	257	550	1223	943	403	455	1113	913	942	846	964	460	322	635	252	263	731
Rb	200	79	135	259	204	162	166	153	196	188	227	200	157	173	343	184	151
Sr	62	116	93	40	81	81	81	62	43	68	41	<100	32	74	6	41	66
Th	11	24	34.2	12	16	75.9	16	27	12	8	15	27.3	25.3	47.8	9	29	16
U	2	1	7.4	8	2	9.6	5	3.4	7	6	2	5.1	4.8	6.4	9	6	1
Zr	211	211	534	359	210	540	278	347	330	320	290	200	73	251	208	249	359
Hf	nd	8	17.5	nd	nd	27.1	12	15.4	nd	13	12	10.90	4.4	13.3	nd	nd	nd
Y	62	44	104	49	34	62	21	76	19	10	5	nd	61	43	5	45	34
Ta	nd	nd	9.4	nd	nd	8.5	nd	6.6	nd	nd	nd	6.1	9.9	7.8	nd	nd	nd
Sc	nd	nd	19.8	nd	nd	36.0	nd	14.2	nd	nd	nd	8.0	1.8	13.4	nd	nd	nd
Ce	172	98	263	136	119	353	174	187	109	103	92	218	29	132	164	102	82
V	5	12	17	18	8	47	16	16	16	20	17	<10	9	28	11	23	26
Cr	9	102	140	136	13	72	101	138	82	123	124	3	165	104	101	93	90
Co	5	0	0.77	5	4	4.6	4	2.2	3	4	2	1.1	0.72	1.9	1	4	5
Ni	5	88	20	8	10	28	7	16	7	7	7	nd	12	18	5	15	19
Cu	4	17	11	8	25	23	4	9	5	2	3	nd	18	13	3	3	9
Zn	32	52	88	101	39	231	70	74	149	70	99	80	37	90	52	73	78
Nb	37	nd	nd	64	47	89	51	nd	57	50	58	nd	nd	55	12	43	49
Ga	22	nd	20	22	25	26	23	22	24	23	23	24	nd	25	25	26	28
F	nd	19	503	nd	nd	nd	nd	296	nd	nd	nd	nd	174	nd	nd	nd	nd
Ratios																	
K/Rb	210	280	285	161	182	197	269	293	203	201	213	205	279	215	142	217	256
Rb/Sr	3.23	0.68	1.38	6.47	2.52	2.00	2.05	2.47	4.56	0.36	5.54	2.05	4.91	2.34	57.20	4.49	2.29
Rb/Ba	0.78	0.14	0.11	0.27	0.51	0.36	0.15	0.17	0.21	0.21	0.24	0.43	0.49	0.27	1.36	0.69	0.21
Y/Nb	1.7	nd	nd	0.76	0.72	0.70	0.41	nd	0.30	0.20	0.09	nd	nd	0.78	0.40	1.05	0.69
Ga/Al	3.1	nd	2.7	3.0	4.0	4.7	3.4	3.0	3.6	3.3	3.3	3.7	nd	4.0	3.8	4.6	6.1
Fe≠	0.93	0.71	0.83	0.89	0.93	0.93	0.81	0.89	0. 0.84	0.89	0.91	1.02	0.88	0.96	0.90	0.96	0.93
Fe/Mg	16.7	27.8	5.42	1.36	2.4	5.41	0.27	9.27	0.92	1.54	1.77	0.76	8.85	28.5	1.56	33.25	14.5

nd: Not determined.
Values of Ce determined by XRF and Ta, Sc values determined by NAA method.
Fe≠ (Fe-number) determined as FeO total.

tremolite–actinolite and relicts of clinopyroxene with minor amounts of biotite, chlorite, epidote, clinozoisite, apatite, titanite and opaques. Metamorphosed diabase differs from dolerite in having more epidote and altered plagioclase. Pyroxenes and plagioclases due to autometamorphism are uralitized and saussuritized, respectively (Mansouri Esfahani et al., 2006). Based on their geochemical features, the diabasic sills/dikes are subalkaline in composition and fall in the high alumina basalts which tectonically are related to Within Plate Alkali field (WPA) (Mansouri Esfahani et al., 2006).

4. Analytical methods

Major and trace elements (including Ce) of highly fresh granitoid rocks were analysed by X-ray fluorescence (XRF) using a Philips PW 2400, following the procedure of Franzini et al. (1975). The analyses were carried out by the Kian Teif Zagros Laboratory in Esfahan, Iran (Table 1).

Nine granitic samples were analyzed for their rare earth elements. The analyses were made by Instrumental Neutron Activation Analysis (INAA) (Terakado et al., 1989) at the Atomic Energy Organization of the Esfahan, Iran Nuclear Technology Center. About 100 mg of the samples were sealed triply in polyethylene bags and irradiated for 1 h at a thermal neutron flux of about 2.8×10^{13} n cm^{-1} s^{-1}, γ-ray spectra and were measured after cooling periods of about 1 and 3 weeks: the counting time of 1.5 h was applied for the former and 3 h for the latter.

The values of Sc and Ta were determined by INAA and the Ce values analyzed by both the XRF and the INAA methods. The values of Ce used in the geochemical diagrams were obtained by XRF method.

For the purposes of this study, the data management, recalculation, plotting and statistical evaluation of the data were facilitated using Newpet (Newpet (c), 1987–1994 Memorial University of Newfoundland Department of Earth Sciences Version: 94.01.07) and the R language package GCDkit (Janoušek et al., 2006).

One specimen of hornblende–biotite granite was coarsely crushed and the amphibole was separated by hand picking and analyzed by X-Ray diffraction method (XRD) with a Philips diffractometer PW1710 at 36 kV and 24 mA using a CU-Kα X-ray tube.

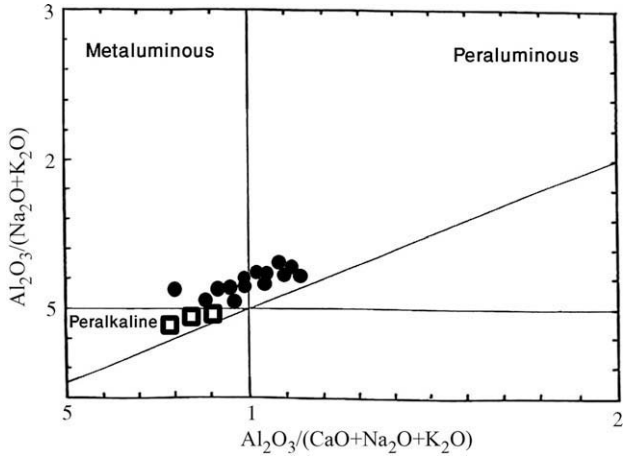

Fig. 4. $Al_2O_3/(CaO + Na_2O + K_2O)$ vs. $Al_2O_3/(Na_2O + K_2O)$ diagram (Maniar and Piccoli, 1989). Note subsolvus granites plot in the field of peraluminous to metaluminous whereas, hypersolvus granites are classified as peralkaline (symbols as in Fig. 3).

5. Geochemistry

5.1. Major and trace elements

Major and trace element concentrations of the Hasan Robat Granite are listed in Table 1. On the average, the subsolvus granites are lower in SiO_2 than the hypersolvus rocks (Table 1). The average content of Al_2O_3 is higher for the former and lower for the latter rocks. The presence of low level of Al_2O_3 as a function of SiO_2 can be ascribed to fractionation of rock-forming silicate minerals. Also, the Na/K ratio, on the average, is less for the subsolvus granites than in the hypersolvus rocks.

Based on the classification of Frost et al. (2001), the rock types of the Hasan Robat Granite are mainly classified as ferroan and alkali–calcic to calc–alkalic. In terms of aluminum saturation index the subsolvus granites are metaluminous to peraluminous composition (Maniar and Piccoli, 1989) (ASI >1), the hypersolvus nature of the granites may be due to fractional crystallization process of subaluminous magma (Zen, 1986). The hypersolvus rocks display weakly peralkaline affinity (Figs. 4 and 5). This is reflected by the lack of sodic amphibole and pyroxene (Frost et al., 2001). The calcic phase in these rocks is ferrohornblende. Furthermore, the studied rocks are characterized by alkali rich with high contents of high field strength elements (HFSE) (e.g. REE, Rb, Ce, Zr, Th, Hf, Nb, and Ta) (Frost et al., 2001). All of these features are the profound characteristics of A-type granite which well exhibited by the Hasan

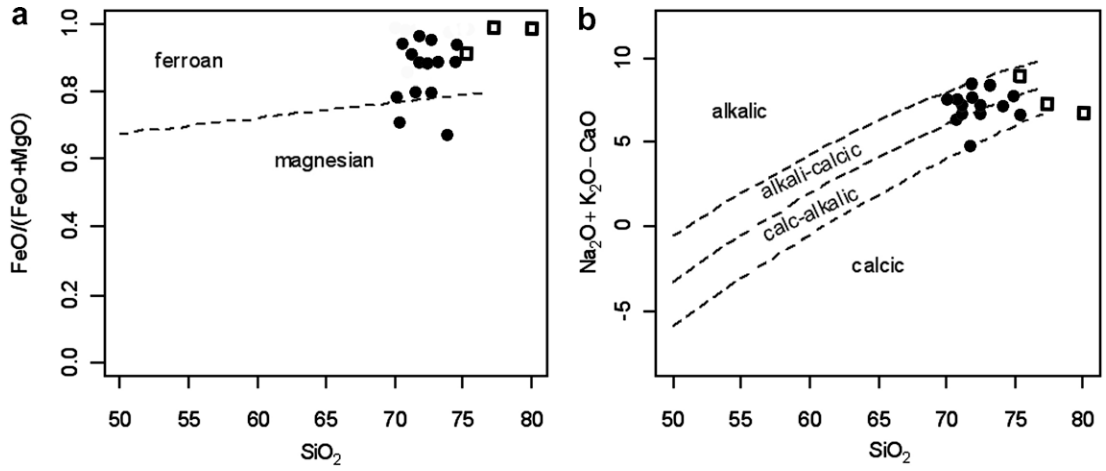

Fig. 5. (a) SiO_2 vs. $Fe^*/(FeO^* + MgO)$ diagram (Frost et al., 2001) for the granites of the Hasan Robat area. Above the Fe^* – line – field of Fe-granitoids corresponding to A-type, below the line, Cordillerian Mg-granites (I-type). (b) SiO_2 vs. $Na_2O + K_2O$–CaO showing fields of alkali–calcic to calc–alkalic for the studied granites (symbols as in Fig. 3).

Robat Granite (c.f. Collins et al., 1982; Whalen et al., 1987; Dall'Agnol et al., 1994, 1999a,b).

On the Harker variation diagrams, it may be observed that most of trace elements (e.g. Rb, Ba, Th, and Nb) of the studied granites decrease with the increase of SiO_2 (Fig. 6). The reduction of Al_2O_3, TiO_2, Zr, Sr and Ba as a function of SiO_2 in the granite may be related to fractional crystallization of mainly biotite, K-feldspar, plagioclase, titanite and zircon (e.g. Jung et al., 2000; Moghazi, 2002; Thuy, 2004; Tatar and Boztug, 2005). The negative Ba anomaly can be taken as an evidence of high temperature feldspar fractionation rather than hornblende and biotite (Rollinson, 1993; Ilbeyli et al., 2004; Arslan and Aslan, 2006).

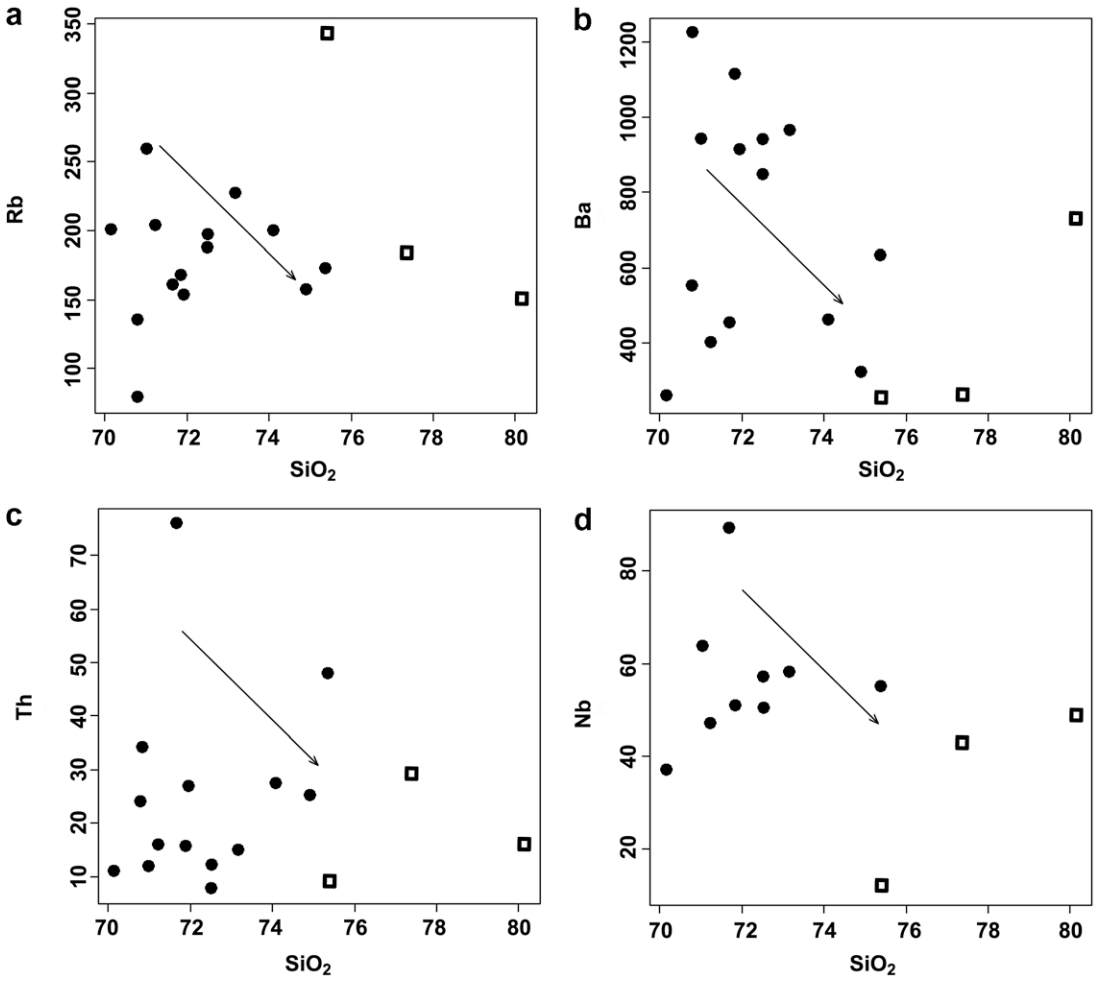

Fig. 6. Selected Harker variation diagrams for the Hasan Robat Granites (symbols as in Fig. 3).

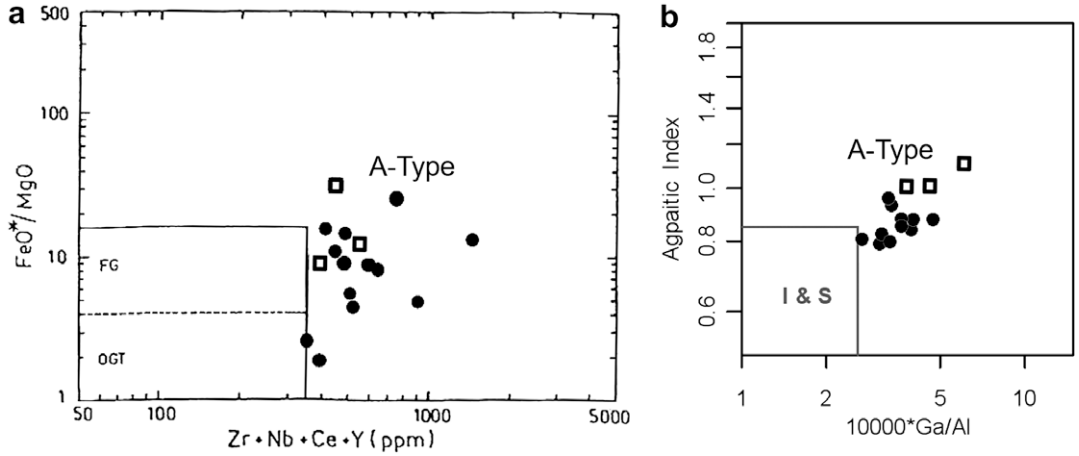

Fig. 7. (a) Zr + Nb + Ce + Y vs. FeO^*/MgO discriminant diagram (Whalen et al., 1987) for the studied granites. All the samples of the Hasan Robat Granites plot outside the FG and OGT fields. OGT: Field for I-, S- and M-type granitoids; FG: field for fractionated I-type granitoids. (b) 10,000*Ga/Al vs. agpaitic index (AI = $Na_2O + K_2O/Al_2O_3$ molar) plot for the Hasan Robat Granite (symbols as in Fig. 3).

Table 2
Rare earth element data for the granitic rocks of the Hasan Robat area.

Sample No.	R13	R22	R7	HR122	HR119	HR113	HR86	HR71	HR22
La	218	112	17.5	252	305	111	103	208	398
Ce	406	212	41.5	471	569	210	192	389	738
Nd	99	64	19	144.5	161	59.5	63	110	229
Sm	26.9	18.4	5.2	31.62	38.7	17.8	14.7	26.2	52.9
Eu	3.35	2.45	0.45	2.49	2.88	2 .40	1.45	2.02	2.61
Gd	4.2	3.9	1.6	5.79	5.8	3.7	<1.5	3.6	7.8
Tb	4.1	3.2	1.19	5.32	5.7	2.99	3.36	3.7	7.9
Dy	nd	nd	nd	nd	nd	nd	14.7	3.7	nd
Tm	1.42	1.10	0.96	1.33	1.49	1.80	0.87	1.19	1.64
Yb	8	7.9	7.4	9.42	9.2	7.5	8	7.5	11.4
Lu	1.6	0.91	1.2	1.49	1.77	0.87	1.1	1.30	2.16
Ratios									
La/Lu	13.88	12.72	1.50	17.44	7.73	13.13	9.63	16.49	18.99
Ba/La	5.60	8.15	18.40	10	11	14.5	4.50	3.05	1.14
Eu/Eu*	0.96	0.87	0.48	0.57	0.58	0.92	0.55	0.63	0.39
∑REEs	1632	942.91	265.14	1953.13	2304.86	854.58	905.39	1571.79	3042.6
LREE/HREE	7.13	5.02	1.49	7.24	8.15	4.66	3.73	7.96	8.26

nd: Not determined.

The value of Ga concentrations ranges from 20 to 26 ppm in the subsolvus granites and from 25 to 28 ppm in the hypersolvus rocks yielding high Ga/Al ratios for both subsolvus (2.7–4.7) and hypersubsolvus rocks (3.8–6.1).

Using (Zr + Nb + Ce + Y) vs. FeO^*/MgO and $10{,}000^*$ Ga/Al vs. agpaitic index (molar $Al = Na_2O + K_2O/Al_2O_3$) diagrams Whalen et al. (1987) found a good discrimination between A-type granites and the M-, I- and S-type. In these diagrams the studied granitoids lie in the A-type field and away from the I- and S-type field boundaries (Fig. 7).

5.2. Rare earth elements

Nine whole rocks were analyzed for their rare earth elements (REE) contents (Table 2) and the data normalized to chondritic values of Thompson (1984) (Fig. 8). The abundances of ∑REE in the Hasan Robat Granite are high (up to 3043 ppm). Fractionation between LREE and HREE (La/Lu = 1.5–19) and the marked Eu anomaly are the profound features of these granitic rocks (Fig. 8a). The high content of middle REE (MREE) (e.g. Sm, Gd) suggests either the precipitation of early formed perthitic feldspar (Bowden and Whitely, 1974) or the crystallization of hornblende (Kochhar, 2000). The chondrite-normalized trace elements pattern of the Hasan Robat Granite displays negative Ba, Sr and Ti and positive Rb, Th, Ce and Zr anomalies (Fig. 8b).

Variations of Ba/La ratios are almost totally controlled by alkali feldspar fractionation. The Y/Nb ratios for the Hasan Robat Granite (except for sample HR24) are low (<1.2). When the granites are plotted on Y/Nb vs. Ba/La diagram (Fig. 9), they define a trend parallel to AF (AF and CPX fractionation trends calculated using partition coefficient of Henderson, 1982). The relative importance of plagioclase vs. alkali feldspar in a fractionation trend can be assessed using the Eu/Eu^* vs. Ba diagram (Fig. 10) (AF–PL trends after Henderson, 1982). This is a further indication that alkali feldspar fractionation may have been involved in the genesis of the Hasan Robat Granite.

6. Petrogenetic remarks

The Hasan Robat Granite (syenogranite, alkali-feldspar granite and rare monzogranite) display petrological and geochemical characteristics typical of A-type granite, as defined by (Loiselle and Wones, 1979). They exhibit subsolvus and hypersolvus mineralogy, an alkaline chemical affinity, low CaO concentration and Iron-enriched. High abundances of Zr, Nb, Ce, Y and high Ga/Al ratio classify these rocks as A-type magma, in the $10{,}000 \times$ Ga/Al vs. (Zr + Nb + Ce + Y) discrimination diagrams (Whalen et al., 1987).

According to several authors (e.g. Emslie and Stirling, 1993; Frost and Frost, 1997; Bonin, 2007) A-type granites are characteristically iron-enriched and commonly considered as being reduced [fO_2 < Fayalite-magnetite-quartz (FMQ)], but there are occurrences of relatively oxidized magnetite-bearing A-type granitoids in the southwestern part of North America (Anderson and Bender, 1989; Anderson and Smith, 1995), in the Amazonian Craton (Magalhaes and Dall'Agnol, 1992; Dall'Agnol et al., 1997a,b, 1999) and elsewhere (Clemens et al., 1986; King et al., 1997).

A number of workers (e.g. Maniar and Piccoli, 1989; Frost and Frost, 1997) have used iron-enrichment to distinguish between granitoids from different tectonic environment. They found that the high Fe-number of ferroan granitoids likely reflect a close affinity to anhydrous reduced basaltic magmas. These magmas are generally hotter and they probably subjected to extensive fractionation toward iron-enrichment and alkali composition (Frost and Frost, 1997). Such conditions commonly occur in extensional environments.

The Fe-number of ferroan granitoid is significantly influenced by the source rocks and the differentiation trends followed by granitic magmas. Osborn (1959) demonstrated that crystallization of anhydrous silicates drives an iron-enriched melt, whereas early magnetite formation precludes iron-enrichment during differentiation. This is particularly well shown by reduced basaltic sources (e.g. tholeiites and alkali basalts) where undergo reduction (e.g. iron-enrichment in the silicates) during differentiation, whereas the relatively oxidizing basaltic rocks related to island arcs do not (Frost and Lindslery, 1991). This indicates that iron-enriched melts come from reduced basaltic rocks (tholeiitic or mildly alkalic) make significant contributions to ferroan granitoids (Frost and Frost, 1997).

The Fe-number is highly affected by the composition of crustal melts particularly those with silica-rich. The ferroan granitoid is predominantly metaluminous, but there are occurrences of peraluminous types (Frost et al., 2001). The peraluminous rocks display a wide range of Fe-number which may be related to differences in source rock composition (Nabelek et al., 1992) as well as the degree of melting (Holtz and Johannes, 1991; Patino Douce and Beard, 1996; Patino Douce and Harris, 1998).

As is the case for some A-type granites the Hasan Robat Granite is known as predominantly ferroan granitoids (Frost et al., 2001; Bonin, 2007) with alkali–calcic to calc–alkalic affinity and high

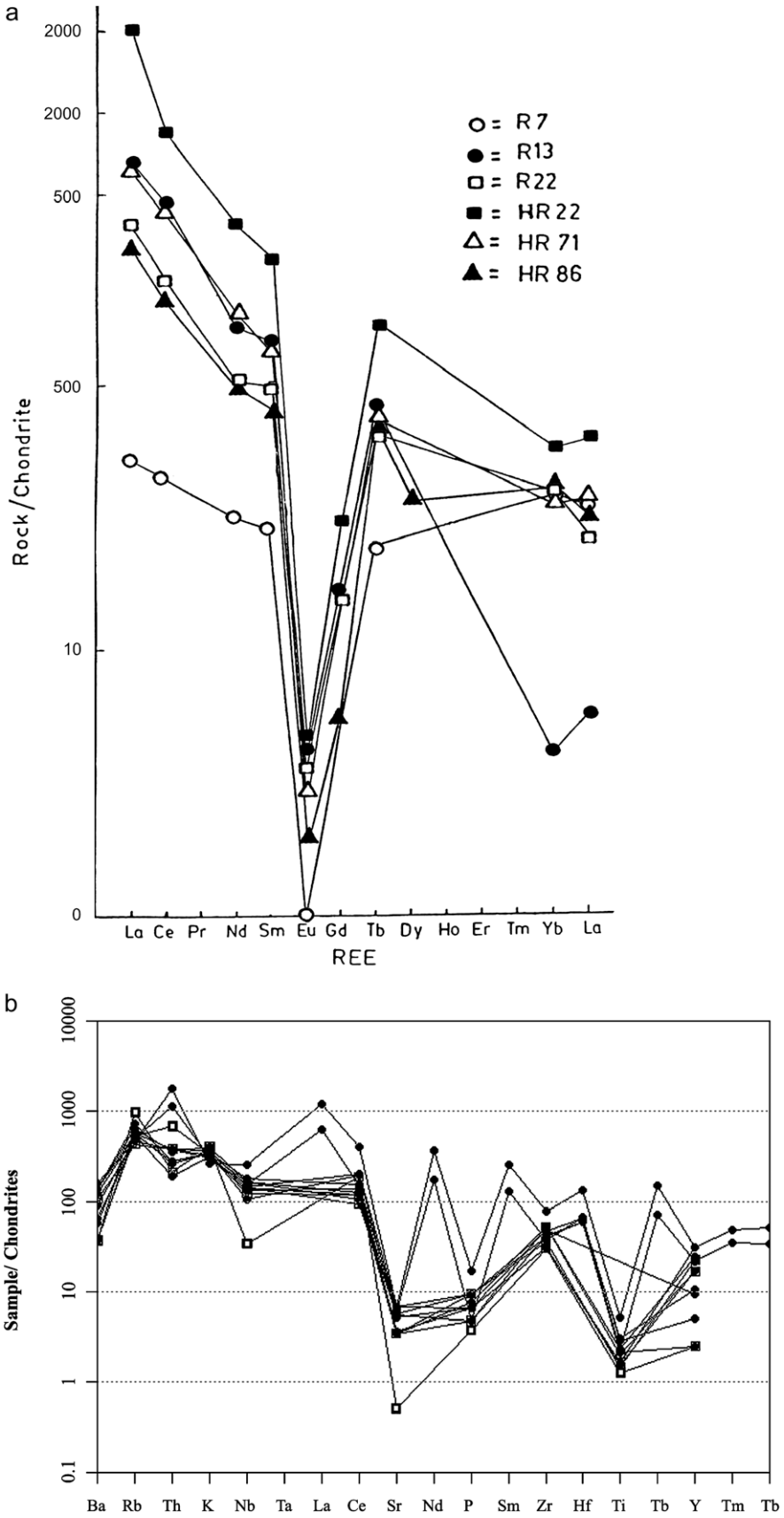

Fig. 8. (a and b) Chondrite normalized REE and trace elements patterns of the representative samples from Hasan Robat Granite. The data of Thompson (1984) were used for normalization.

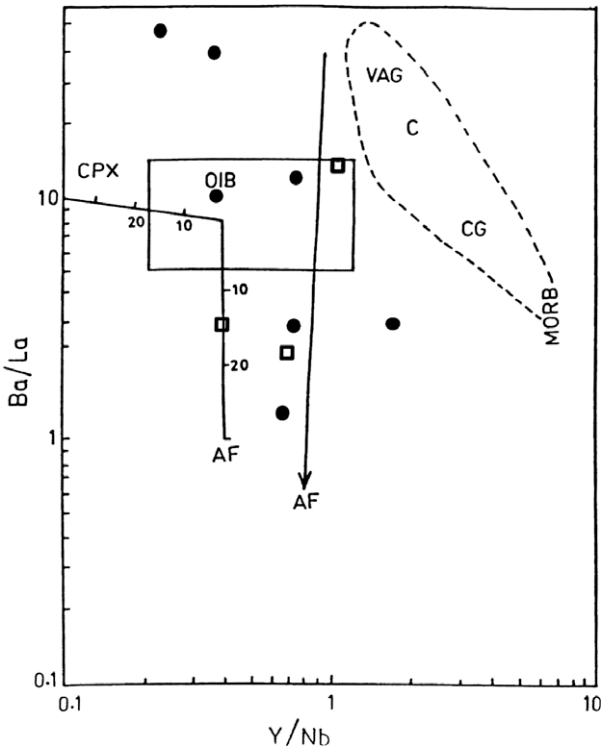

Fig. 9. Y/Nb vs. Ba/La diagram showing fractionation of alkali feldspar (AF) trend for the granites of the Hasan Robat area. (AF and CPX fractionation trends calculated using partition coefficient of Henderson, 1982). (the OIB field refers to the Oceanic Island Basalt samples which are clearly fractionates of mantle derived magma) (symbols as in Fig. 3).

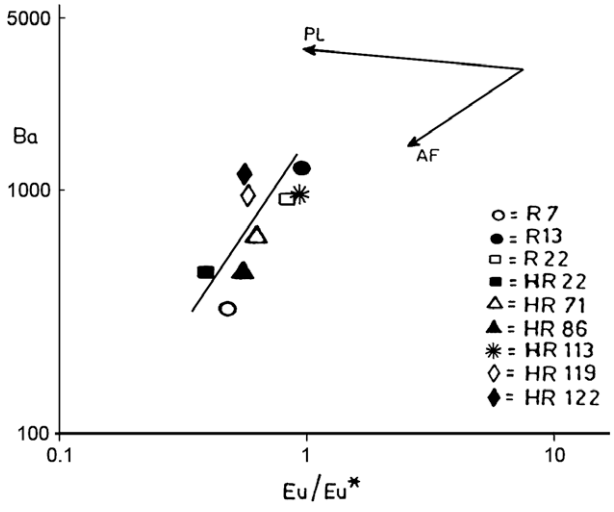

Fig. 10. Eu/Eu* vs. Ba plot for the granite of Hasan Robat area. AF and PL are Reyleigh fractionation trends calculated for removal of alkali feldspar (AF) and plagioclase feldspar (PL). (AF–PL trends calculated after Henderson, 1982).

Fe/(Fe + Mg). Also, the Y/Nb data obtained for these rocks ranges from 0.09 to 1.7 with the average value of 0.89 reflecting a mantle origin for A-type magma (Eby, 1992). When the data are applied to Y/Nb vs. Ba/La diagram, they plot either within the Oceanic Island Basalt (OIB) field (Fig. 9) or along differentiation trends emanating from this field (Eby, 1990). Using the Nb–Y–Ce ternary diagram (Eby, 1992) the data clearly lie in the mantle A-type field (A_1 granite) (Fig. 11). Such geochemical characteristics suggest that the

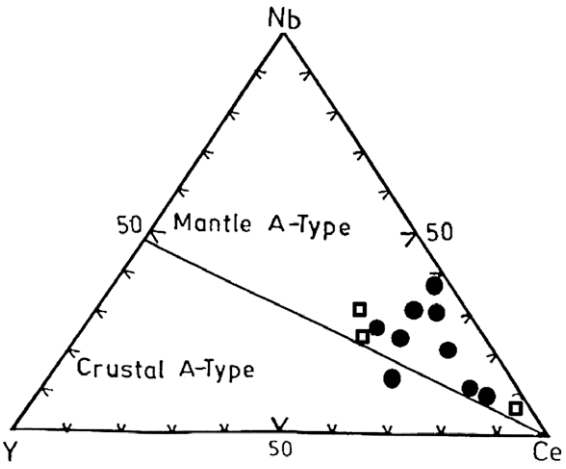

Fig. 11. The Hasan Robat granitic rocks in the Nb–Ce–Y discrimination plot (Eby, 1992). Note most of the samples fall in the mantle A-type field (symbols as in Fig. 3).

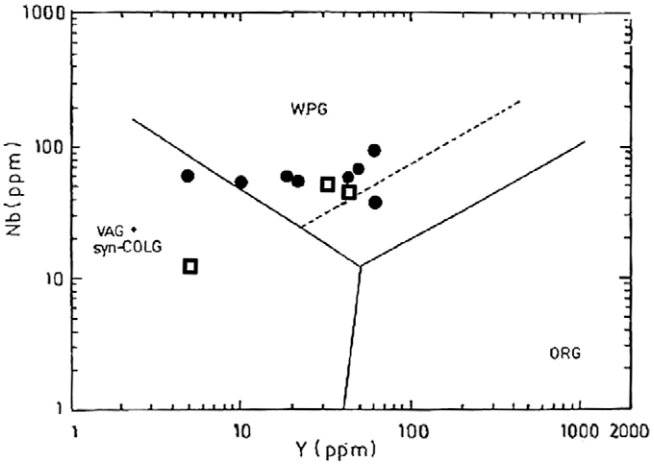

Fig. 12. Y vs. Nb diagram (Pearce et al., 1984) for the granitic rocks of the Hasan Robat area. Note most of the granites lie in the Within Plate Granite field (symbols as in Fig. 3). SYN-COLG: SYN-COLLISON GRANITES, WPG: WITHIN PLATE GRANITES, VAG: VOLCANIC ARC GRANITES, ORG: OCEANIC RIDGE GRANITES.

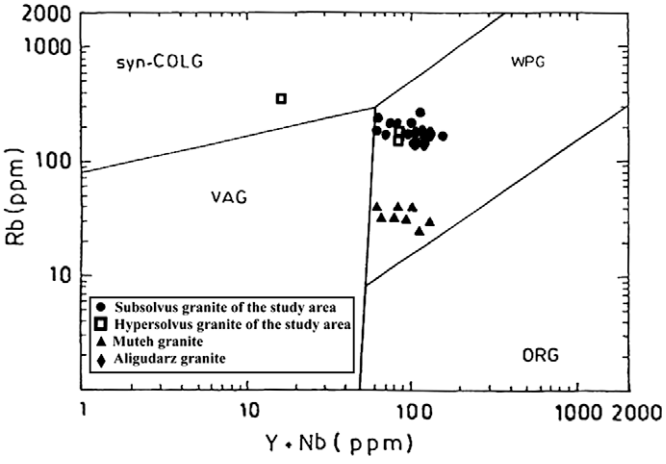

Fig. 13. Y + Nb vs. Rb diagram (Pearce et al., 1984) of the granitic rocks of the Hasan Robat, Muteh, and Aligudarz areas. Note most of the granites cluster in the WPG field.

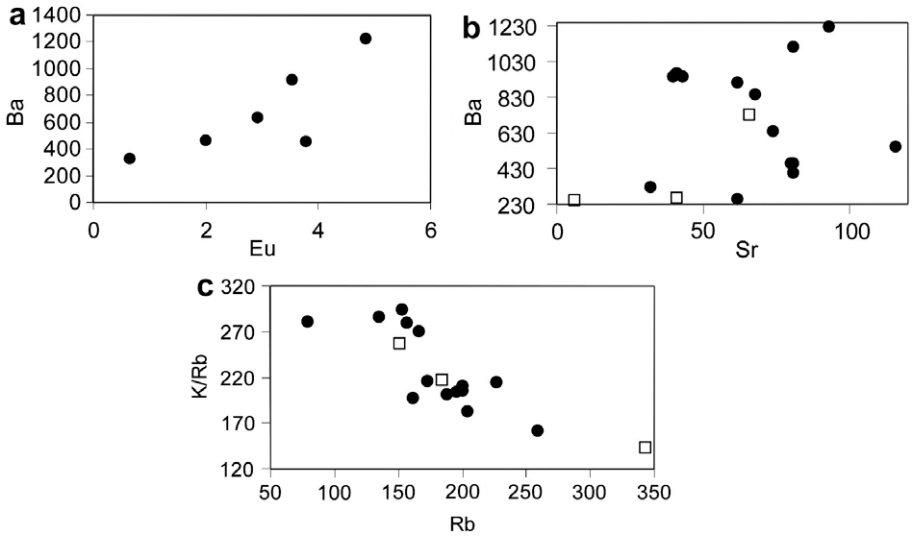

Fig. 14. (a) Eu vs. Ba, (b) Sr vs. Ba, and (c) Rb vs. K/Rb plot for the granites of the Hasan Robat area (symbols as in Fig. 3).

suite are obviously fractionations of mantle derived magmas (e.g. Eby, 1992; Beyth et al., 1994b; Whalen et al., 1996; Kessel et al., 1998; Volkert et al., 2000; Mushkin et al., 2003; Vernon, 2004; Saleh, 2006) likely crystallized under reduced to relatively oxidized conditions in an extensional environment. On the base of Nb vs. Y and Rb vs. Y + Nb diagrams (Pearce et al., 1984), the Hasan Robat Granite and several other granitic bodies (e.g. Muteh and Aligudarz Granites which are located in 23 km northwest and 85 km west of the Hasan Robat Granite, respectively) (Sharifi, 1997; Bagheri, 2001) lying in the vicinity of the study area, classified as WPG (Figs. 12 and 13).

Exposures of the diabase sills/dikes in the Hasan Robat Granite are small. Except for these rocks, any clear mantle signature is lacking. Kessel et al. (1998) found out that mafic dikes are the source rocks from which A-type granitic rocks in the Arabian–Nubian Shield are derived. Uncertainties remain whether the studied sills/dikes can be the parents from which the Hasan Robat Granite was originated. Access to much more geochemical data will undoubtedly lead to further information regarding the source rocks of the studied granite.

7. Summary and conclusion

The Late-Precambrian alkaline to peralkaline magmatic suite of the Hasan Robat area (NW of Esfahan, Iran) is composed of syenogranite, alkali-feldspar granite, and minor monzogranite. The Hasan Robat Granite displays several mineralogical and geochemical features typical of A-type granitoid rocks as explained by Loiselle and Wones (1979), notably the presence of cogenetic subsolvus to hypersolvus granites mostly with perthitic, rapakivi textures, and features of ferroan and alkali–calcic to calc–alkalic. In terms of aluminous saturation, the suite is metaluminous to peraluminous with minor of peralkaline nature. Most of the studied rocks are felsic with high SiO_2, Fe/Mg, total alkali (K_2O, Na_2O), Zr, Nb, Y, Hf, Ta, Ga/Al, REE, and low contents of MgO, CaO, P_2O_5, and Sr. The rare earth elements chondrite-normalized pattern of the Hasan Robat Granites exhibits that the two rock types have similar contents of REE being enriched in LREE with moderately depleted in HREE and negative Eu anomaly (Fig. 8a).

Plagioclase fractionation would produce negative Sr and Eu anomalies. However, Eu depletion could also be produced by potassium feldspar fractionation, which would explain the negative Ba anomaly (Xu et al., 2007). The plots of Eu and Sr vs. Ba, correlate positively (Fig. 14a and b) indicating that fractional crystallization plays an important role in magmatic evolution. Moreover, fractionation of K-feldspar likely caused an increase in Rb and decrease in both Sr and Ba, accompanied by a decrease in K/Rb ratio (Fig. 14c). Collins et al. (1982) point out that the subtle, regular variations over a limited SiO_2 (between 60 and 80 wt.%) interval of certain elements such as Ce, Zr, Zn, Y, Nb, Ga and elemental ratios (e.g. K/Rb) within A-type suites are in favor of fractional crystallization. In order to determine the role of fractional crystallization in the magmatic evolution, Rb and Sr are plotted on Rb vs. Sr diagram (Fig. 15). The Rb–Sr trend of the studied granitic rocks is not adequately reproduced by batch partial melting

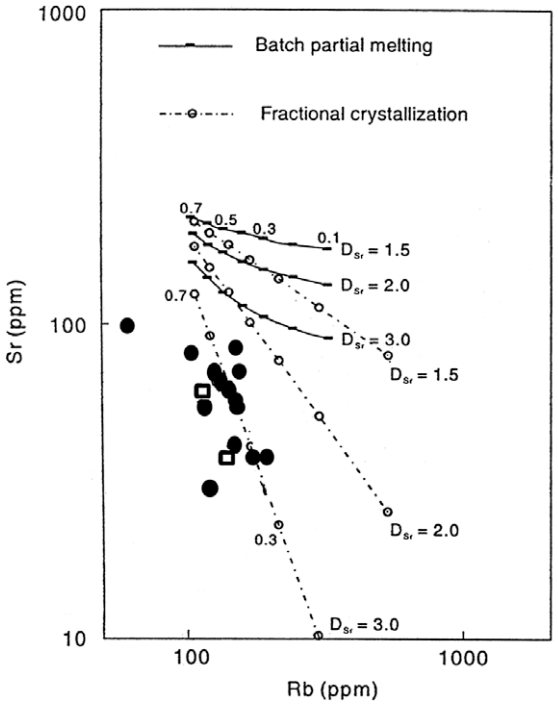

Fig. 15. Rb vs. Sr diagram (Xu et al., 2007) for granitic rocks of the Hasan Robat area. Curves show the batch partial melting and fractional crystallization models for three different D_{Sr}. Numbers along curves refer to the degree of partial melting and the degree of crystallization (Xu et al., 2007) (symbols as in Fig. 3).

(Fig. 15), even by varying D_{Sr} (between 1.5 and 3), whereas, it shows better fit for fractional crystallization. The plotting of the granitic rocks on the Y/Nb vs. Ba/La and Eu/Eu* vs. Ba diagrams show that alkali feldspar fractionation has been responsible for the magmatic evolution of the studied rocks (Figs. 9 and 10).

The high Fe-number of ferroan granites of the Hasan Robat Granite likely manifests derivation from anhydrous reduced basaltic magmas. Crystallization of such magmas derives an iron-enrichment (Osborn, 1959) and alkali composition melt (Frost et al., 2001). Such conditions are favorable in an extentional environment (Frost et al., 2001). The primary melt for the A-type Hasan Robat Granite is probably an anhydrous alkaline mafic magma which is similar in composition to the high alumina basalt nature of the exposed sills/dikes.

Based on the overall observations, the generation of the Hasan Robat Granite may be outlined in terms of two-stage model. The first stage is characterized by mantle-derived parental mafic magmas emplaced in a deep crustal level. During their ascent, these magmas possibly have subjected to limited fractionation and probably minor contamination by crustal material. In the second stage, the fractionation of the mafic magmas in the magma chamber produced the more felsic members of the suite.

Acknowledgments

The present work forms a part of Ph.D thesis submitted to Panjab University, Chandigarh, India. I am greatly indebted to the Chairman, CAS (Centre of Advanced Study) in Geology, Panjab University, Chandigarh for extending all the facilities to carry out the present work. The manuscript was significantly improved by the critical comments of anonymous reviewers to whom the authors are grateful.

References

Alavi, M., 1994. Tectonics of the Zagros orogenic belt of Iran: new data and interpretations. Tectonophysics 229, 211–238.

Anderson, J.L., Bender, E.E., 1989. Nature and origin of Proterozoic A-type granitic magmatism in the southwestern United States of America. Lithos 23, 19–52.

Anderson, J.L., Smith, D.R., 1995. The effects of temperature and fO_2 on the Al-in-hornblende barometer. American Mineralogist 80, 549–559.

Arslan, M., Aslan, Z., 2006. Mineralogy, petrography and whole-rock geochemistry of the Tertiary granitic intrusions in the Eastern Pontides, Turkey. Journal of Asian Earth Sciences 27, 177–193.

Bagheri, N., 2001. Petrology, geochemistry and rare earth elements of the granitoids of the west of Golpaygan with emphasis on their enclaves. M.Sc. Thesis, Isfahan University, Iran, 107 p. (in Farsi).

Bagherian, S., Khakzad, A., 2001. Petrogenesis of granitoid massif of Molataleb area (North Aligudarz). Scientific Quarterly Journal 10 (41–42), 79–82.

Beyth, M., Stern, R.J., Altherr, R., Kroener, A., 1994. The late Precambrian Timna igneous complex, southern Israel: evidence for comagmatic-type sanukitoid monzodiorite and alkali granite magma. Lithos 31, 103–124.

Bonin, B., 2007. A-type granites and related rocks: evolution of a concept, problems and prospects. Lithos 97, 1–29.

Bowden, P., Whitely, J.E., 1974. Rare earth patterns in peralkaline and associated granites. Lithos 7, 15–21.

Clemens, J.D., Holloway, J.R., White, A.J.R., 1986. Origin of an A-type granite: experimental constrains. American Mineralogist 71, 317–324.

Collins, W.J., Beams, S.D., White, A.J.R., Chappell, B.W., 1982. Nature and origin of A-type granites with particular reference to southeastern Australia. Contribution to Mineralogy and Petrology 80, 189–200.

Dall'Agnol, R., Lafon, J.M., Macambira, M.J.B., 1994. Proterozoic anorogenic magmatism in the central Amazonian Province, Amazonian craton: geochronological, petrological and geochemical aspects. Mineralogy and Petrology 50, 113–138.

Dall'Agnol, R., Pichvalant, M., Champenois, M., 1997a. Iron–titanium oxide minerals of the Jamon granite, Estern Amazonian region, Brazil: implications for the oxygen fugacity in Proterozoic, A-type granites. Anais da Brasileira de Ciencias 69, 325–347.

Dall'Agnol, R., Ramo, O.T., Magalhaces, M.S., Macambria, M.J.B., 1997b. Archean granitoids as magma sources for the anorogenic Paleoproterozoic Jamon and Musa granites (Eastern Amazonian Craton): new constraints based on geochemical and Sm–Nd isotope data. In: South American Symposium an Isotope Geology. Extended Abstracts. Campos do Jordao: CPGEO-IG-USP, pp. 96–97.

Dall'Agnol, R., Scaillet, B., Pichavalant, M., 1999. An experimental study od a lower Proterozoic A-type granite from thee Eastern Amazonian Craton, Brazil. Journal of Petrology 40 (11), 1673–1698.

Dall'Agnol, R., Magalhaes, M.S., Teixeira, N.P., 1999a. Rapakivi granites from Brazil and adjacent areas. Precambrian Research 95, 9–39.

Dall'Agnol, R., Ramo, O.T., Magalhaes, M.S., Macambira, M.J.B., 1999b. Petrology of the anorogenic, oxidized Jamon and Musa granite, Amazonian craton: implications for the genesis of Proterozoic A-type granites. Lithos 46, 431–462.

Davoudian, A.R., Hamadani, A., Shabanian, N., Makizadeh, M.A., 2007. Petrological and geochemical constrains on the evolution of the Cheshmeh-Sefid granitoid complex of Golpayegan in the Sanandaj–Sirjan Zone, Iran. Neues Jahrbuch Fur Mineralogie-Abhandlungen 184, 117–129.

Eby, G.N., 1990. The A-type granitoids: a review of their occurrence and chemical characteristics and speculations on their petrogenesis. Lithos 26, 115–134.

Eby, G.N., 1992. Chemical subdivision of the A-type granitoids: petrogenetic and tectonic implications. Geology 20, 641–644.

Emslie, R.F., Stirling, J.A.R., 1993. Rapakivi and related granitoidsof the Nain plutonic suite: geochemistry, mineral assemblages and fluid equilibria. Canadian Mineralogist 31, 821–847.

Franzini, M., Leoni, L., Saitta, M., 1975. Revisione di una metodologia analitica per fluorescenza-X basata sulla correzionecompleta sugli effetti di matrice. Rendiconti della Societa Italiana di Mineralogiae Petrologia 31, 356–378.

Frost, C.D., Frost, B.R., 1997. High-K, iron-enriched rapakivi-type granites: the tholeiite connection. Geology 25, 647–650.

Frost, B.R., Lindslery, D.H., 1991. The occurrence of Fe–Ti oxides in igneous rocks. In: Linslery, D.H. (Ed.), Oxide Minerals: Petrologic and Magmatic Significances, vol. 25. Mineralogicasl Society of America, Reviewers in Mineralogy, pp. 433–486.

Frost, B.R., Barnes, C.G., Collins, W.J., Arculus, R.J., Ellis, D.J., Frost, C.D., 2001. A geochemical classification for granitic rocks. Journal of Petrology 42 (11), 2033–2048.

Henderson, P., 1982. Inorganic Geochemistry. Pergamon, Oxford. 312 p..

Holtz, F., Johannes, W., 1991. Genesis of peraluminous granites I. Experimental investigation of melt compositions at 3 and 5 kb and various H_2O activities. Journal of Petrology 32, 935–958.

Ilbeyli, N., Pearce, J.A., Thirlwall, M.F., Mitchell, J.G., 2004. Petrogenesis of collision-related plutonics in Central Anatolia, Turkey. Lithos 72, 163–182.

Janoušek, V., Farrow, C.M., Erban, V., 2006. Interpretation of whole-rock geochemical data in igneous geochemistry: introducing geochemical data toolkit (GCDkit). Journal of Petrology 47, 1255–1259.

Jung, S., Hoernes, S., Mezger, K., 2000. Geochronology and petrogenesis of Pan-African, syn-tectonic, S-type and post-tectonic A-type granite (Namibia): products of melting of crustal sources, fractional crystallization and wall rock entrainment. Lithos 50, 259–287.

Kessel, R., Stein, M., Navon, O., 1998. Petrogenesis of late Neoproterozoic dikes in the northern Arabian–Nubian Shield: implications for the origin of A-type granites. Precambrian Research 92, 195–213.

Khalili, K., Khalili, M., 2002. Kolah-Ghazi granodiorites enclaves of south Esfahan. Abstracts of 20th Symposium of Geosciences, Iran, pp. 123–124.

King, P.I., White, A.J.R., Chappell, B.W., Allen, C.M., 1997. Characterization and origin of aluminous A-type granites from the Lachlan fold belt, southeastern Australia. Journal of Petrology 38, 371–391.

Kochhar, N., 2000. Attributes and significance of the A-type Malani magmatism, northwestern Peninsular India. In: Deb, M. (Ed.), Crustal Evolution and Metallogeny in the Northwestern India Shield, vol. 9. Narosa, New Delhi, pp. 158–188.

Loiselle, M.C., Wones, D.I., 1979. Characteristics and origin of anorogenic granites. Geology Society America, Abstract with Programs 11, 468 p.

Magalhaes, M.S., Dall'Agnol, R., 1992. Estudos de minerais opacos e susceptibilidade magnetica nos granitos Musa e Jamon (regiao de Rio Maria-SE do Para) e suas implicacoes petrologicas. Revista Brasileira de Geociencias 22, 184–197.

Maniar, P.D., Piccoli, P.M., 1989. Tectonic discrimination of granitoids. Geological Society American Bulletin 101, 635–643.

Mansouri Esfahani, M., 2003. Petrology of Hasan Robat Granite and associated rocks, Northwest of Esfahan, Central Iran, Ph.D. Thesis, Panjab University India, 225 p.

Mansouri Esfahani, M., Khalili, M., 2007. Petrography and geochemistry of the xenoliths and enclaves in the Hasan Robat Granite, NW Esfahan, Iran. In: Abstract of 9th International Conference of Jordanian Geologist's Association 73.

Mansouri Esfahani, M., Kochhar, N., Khalili, M., Gupta, L.N., 2006. Petrography and geochemistry of diabase sills/dikes in the Hasan Robat area, NW Esfahan, Iran. Bulletin of the Indian Geologist's Association 39, 11–18.

Moazzen, M., Moayyed, M., Modjarrad, M., Darvish, E., 2004. Azna granitoid as an example of syn-collision S-type granitization in Sanandaj–Sirjan metamorphic belt, Iran. Neues Jahrbuch Fur Mineralogie-Abhandlungen 11, 489–507.

Moghazi, A.M., 2002. Petrology and geochemistry of Pan-African granitoids, Kab Amiri area, Egypt-implications for tectonomagmatic stages in the Nubian shield evolution. Mineralogy and Petrology 75, 41–76.

Mushkin, A., Navon, O., Halicz, L., Hartmann, G., Stein, M., 2003. The petrogenesis of A-type magmas from the Amram massif, southern Israel. Journal of Petrology 44 (5), 815–832.

Nabelek, P.I., Russ-Nabelek, C., Denison, J.R., 1992. The generation and crystallization conditions of the Proterozoic Harney Peak leucogranite, Black Hills, South Dakota. USA: petrologic and geochemical constraints. Contributions to Mineralogy and Petrology 110, 173–191.

Noghreian, M., Tabatabaei-Manesh, S.M., 1995. A study of Kolah-Ghazi granitoid with emphasize on its contact metamorphism (in Farsi with English abstract). Geosciences Quarterly, GSI 4 (17–18), 60–76.

Osborn, F.F., 1959. Role of oxygen pressure in the crystallization and differentiation of basaltic magma. American Journal of Science 257, 609–647.
Othrody, S., 1988. Study of petrology and petrography of the Muteh granitic masses. Unpublished, M.Sc. Thesis, Tehran University, Iran 152 p. (in Farsi).
Patino Douce, A.F., Beard, J.s., 1996. Effects of $Pf O_2$ and Mg/Fe ratio on dehydration melting of model metagrawackes. Journal of Petrology 37, 999–1024.
Patino Douce, A.F., Harris, N., 1998. Experimental constraints on Himalayan anatexis. Journal of Petrology 39, 689–710.
Pearce, J.A., Harris, N.B.W., Tindle, A.G., 1984. Trace element discrimination diagrams for the tectonic interpretation of granitic rocks. Journal of Petrology 25, 956–983.
Rashidnejad-Omran, N., Emami, M.H., Sabzehei, M., Rastad, E., Bellon, H., Pique, A., 2002. Lithostratigraphie et historie Paleozoique a Paleocene des complexes metamorphiques de la region de Muteh, zone de Sanandaj–Sirjan (Iran meridional). Comptes Rendus Geoscience 334, 1185–1191.
Rollinson, H., 1993. Using Geochemical Data: Evolution, Presentation, Interpretation. Longman Scientific & Technical, UK. 344 p..
Saleh, G.M., 2006. Pan-African younger granitoids of the southern eastern desert, Egypt. Geology, geochemical constraints, and mineralization. International Geology Review 48, 360–381.
Sepahi, A.A., Athari, S.F., 2006. Petrology of major granitic plutons of the northwestern part of the Sanandaj–Sirjan Metamorphic Belt, Zagros orogen, Iran: with emphasis on A-type granitoids from the SE Saqqez area. Neues Jahrbuch Fur Mineralogie-Abhandlungen 183, 93–106.
Shabanian, N., Khalili, M., Davoudian, A.R., Mohajjel, M., 2009. Petrography and geochemistry of mylonitic granite of Ghaleh-Dezh, NW Azna, Sanandaj–Sirjan Zone, Iran. Neues Jahrbuch fur Mineralogie Monatshefte/Abhandlungen 185 (3), 233–248.
Sharifi, M., 1997. Geology and petrology of metamorphic and igneous rocks in the NE of Golpaygan area. M.Sc. Thesis, Isfahan University, Iran 258 p. (in Farsi).
Streckeisen, A., 1979. Classification and nomenclature of volcanic rocks, lamprophyre, carbonatites and melilitic rocks: recommendations and suggestions of IUGS sub-commission on the systematics of igneous rocks. Geology 7, 331–335.
Tabatabaei-Manesh, S.M., 1994. A study of geology and petrology of Kolah-Ghazi intrusive body (south and southeast of Esfahan) M.Sc. Thesis, Isfahan University, Iran 275 p. (in Farsi).
Tahmasebi, Z., 2009. Petrology and geochemistry of the Astaneh granitoid (SW of Arak), Ph.D. Thesis, Isfahan University, Iran.
Tatar, I., Boztug, D., 2005. The syn-collisional Danaciobasi biotite leucogranite derived from the crustal thickening in central Anatolia (Kirikkale), Turkey. Geological Journal 40, 571–591.
Terakado, Y., Fujitani, T., Takado, J., 1989. Precise determination of rare earth elements in rocks by neutron activation analysis: a preirradiation group separation method and a problem concerning granitic rock analysis. Journal of Radioanalytical and Nuclear Chemistry 129, 23–31.
Thiele, O., Alavi, M., Assefi, R., Hushmand-Zadeh, A., Seyed-Emami, K., Zahedi, M., 1968. Explanatory text of the Golpayegan quadrangle Map 1: 250, 000. Geology Survey of Iran E7, 1–24.
Thompson, R.N., 1984. Dispatches from the basalt front. 1. Experiments. Proceeding Geological Association 95, 249–262.
Thuy, N.T.B., 2004. Geochemical and isotopic constraints on the petrogenesis of granitoids from the Dalat zone, southern Vietnam. Journal of Asian Earth Sciences 23, 467–482.
Turkian, A., 2008. Magmatism investigation of the intrusive body in south of Qorveh area, Sanandaj. Ph.D. Thesis, Isfahan University, Iran, 145 p.
Vernon, R.H., 2004. A practical Guide to Rock Microstructure. Cambridge University Press, 594 pp.
Volkert, R.A., Feigenson, M.D., Patino, L.C., Delaney, J.S., Drak Jr., A.A., 2000. Sr and Nd isotopic compositions, age and petrogenesis of A-type granitoids of the Vernon Supersuite. NewJersey Highlands, USA. Lithos 50, 325–347.
Whalen, J.B., Currie, K.L., Chappell, B.W., 1987. A-type granites: geochemical characteristics, discrimination and petrogenesis. Contribution to Mineralogy and Petrology 96, 407–419.
Whalen, J.B., Jenner, G.A., Longstaffe, F.J., Robert, F., Gariepy, C., 1996. Geochemical and isotopie (O, Nd, Pb and Sr) constraints on A-type granite: petrogenesis based on the Topsail igneous suits, Newfoundland Appalachians. Journal of Petrology 37, 1463–1489.
Xu, C., Huang, Z., Qi, L., Fu, P., Liu, C., Li, E., Gung, T., 2007. Geochemistry of Cretaceous granites from Mianning in the Panix region, Sichuan Province, southwestern China: implications for their generation. Journal of Asian Earth Sciences 29, 737–750.
Zen, E.-An., 1986. Aluminum enrichment in silicate melts by fractional crystallization: some mineralogic and petrographic constraints. Journal of Petrology 27 (Part 5), 1095–1117.